Transportation Research Interdisciplinary Perspectives 14 (2022) 100603

Contents lists available at ScienceDirect

Transportation Research Interdisciplinary Perspectives

journal homepage: www.elsevier.com/locate/trip

Feasibility study for the estimation of a motorcycle helmet Centre of Gravity accelerations with 6 Degrees of Freedom (6DOF) system

A. Bracali *, D. Barbani, N. Baldanzini

Department of Industrial Engineering, University of Florence, Firenze, Italy

ARTICLE INFO

Keywords:
Traumatic Brain Injuries (TBIs)
Head acceleration
Helmet acceleration
Safety
Smart helmet

ABSTRACT

Traumatic Brain Injury (TBIs) is the most frequent cause of serious and fatal road crashes. European Community has adopted an automatic emergency call system (eCall) and made it mandatory for new cars since 2018. eCall was adapted also to motorcycles, which are worldwide linked to significant mortality and trauma rates in crashes. In this context, the development of a helmet fitted with sensors, capable to estimate biomechanical crash consequences and to transmit the information over the eCall system, has the potential to reduce motorcycle crashes severity. The aim of this study is to adapt the 6 Degrees of Freedom (6DOF) method to the estimation of the linear and rotational accelerations of a helmet Centre of Gravity (CoG) during an impact and check the fitness of the method for the scope. The research was performed with virtual testing tools, reproducing three impacts of the helmet on a deformable structure at 8 m/s. The results indicate that the 6DOF estimates the peak values of the linear acceleration components with good approximation, while the peak values of the rotational acceleration components and the time histories of all the components present large errors. The 6DOF cannot be extended beyond the application to rigid bodies and another prediction method has to be identified for the accelerations of the helmet centre of gravity.

1. Introduction

Motor vehicle crashes are among the most common causes of Traumatic Brain Injuries (TBIs)-related death, behind only intentional self-harm and unintentional falls. In the USA, these three principal mechanisms of injury account respectively for 18.7%, 32.5% and 28.1% of all injuries (Centers for Disease Control and Prevention et al., 2014). A study made on 1557 TBI patients (Majdan et al., 2012) hospitalized in Austria, Slovakia, Bosnia, Croatia and Macedonia highlighted that 44% of TBIs were traffic related (car drivers, car passengers, motorcyclists, bicyclists and pedestrians). Several studies pointed out that among all road users, TBIs are mainly linked to motorcyclists with fatal and serious injuries (Chinn et al., 2001; Gibson and Thai, 2007; Aare and Holst, 2003; Meng et al.). These studies highlighted the importance of the investigation of brain trauma in motorcyclists and the development of new methods to mitigate these injuries.

Usually, TBI risk assessment is performed with criteria comprised of a biomechanical metric and an injury risk function. Most of the existing biomechanical metrics are based on head kinematics, measured with crash test dummies or instrumented headforms. Injury criteria based on linear acceleration were the first ones to be developed, e.g. Head Injury Criterion (HIC) (Versace, 1971), a metric for head injuries widely used also in Euro NCAP testing Protocols (EuroNCAP, 2017a,b). More recent studies identified the rotational acceleration as the main cause of TBIs (Gennarelli et al., 1972; Thomas et al., 1982; Melvin, 1991; Kleiven, 2006). The latter findings triggered the development of new injury criteria based on the rotational movement of the brain. The most common ones are: Generalized Acceleration Model for Brain Injury Threshold (GAMBIT) (Newman, 1986), Head Injury Power (HIP) (Newman et al., 2000) and Brain Injury criteria (BrIC) (Takhounts et al., 2003). Applications range from the estimation of the level of trauma in accident reconstruction to vehicle homologation, using sensors of anthropometric test dummies. All these criteria may also be used to estimate injuries directly in real world crashes, but their application is hampered by the technological limits in performing a precise and accurate estimation of the kinematic data (linear and rotational accelerations).

Helmets are currently widely used as protective devices to mitigate the severity of TBIs caused by an impact. Several systems incorporate micro-electromechanical systems (MEMS) inertial sensors into helmets, to measure some kinematic data and to estimate linear and rotational head accelerations at the Centre of Gravity (CoG) of the head. Head Impact Telemetry System (HITS) (Chu, 2005) was one of the earliest and most widely used device to collect kinematic data in the sport field (S.M. et al., 2005; Funk et al., 2007; Greenwald et al., 2008; Crisco

* Corresponding author.
E-mail address: andrea.bracali@unifi.it (A. Bracali).

https://doi.org/10.1016/j.trip.2022.100603
Received 30 September 2021; Received in revised form 15 February 2022; Accepted 13 April 2022

et al., 2011; Beckwith et al., 2012; Rowson et al., 2012; Jadischke et al., 2013). This device is comprised of an array of 6 single-axis accelerometers, a data acquisition system, an on-board memory and a wireless transceiver; each accelerometer is embedded in a fabric padding physically attached to the helmet padding. This insert acts as a spring maintaining the essential contact between head and the accelerometers during an impact. The axes of the accelerometers are orthogonally oriented towards the head surface. Their function is to primarily measure the linear acceleration of the head, instead the rotational acceleration is estimated assuming a hypothetical pivot point in the neck.

HITS was updated, reorienting the sensing axes of the accelerometers tangentially to the head surface and adding six single-axis accelerometers for a total of twelve sensors. The new system, named 6DOF measurement device (Rowson et al., 2011), estimates both the linear and the rotational accelerations iteratively solving an optimization problem (Beckwith et al., 2007; Kimpara et al., 2011; Rowson et al., 2012). HITs and 6DOF are the most common systems for monitoring head kinematics and in both of them the sensing elements need to be in contact with the head to obtain accurate results.

More recently the gForce Tracker (GFT) (Allison et al., 2015) was developed. This system is characterized by one triaxial accelerometer and one triaxial gyroscope embedded inside a casing attached to a helmet. This technology provides only the maximum values of the resultant linear acceleration and rotational velocity obtained from a power fit regression and this data is not enough to perform an estimation of the head injuries.

Another category of devices, rigidly connected to the head but not associated to a helmet, comprises mount-guards (Miller et al., 2018; Gabler et al., 2020), earplugs (Knox, 2002) and bands (Tierney et al., 2008). These devices provide more detailed and accurate data, but they are hardly acceptable by riders (i.e. motorcycle or scooter users) for daily usage. In fact, a behavioural change would be required to adopt these devices, but previous research projects such as SAFERIDER (Bekiaris et al., 2009) or RiderScan (Delhaye and Marot, 2015) proved that riders are reluctant to change habits. The outcomes of the previously mentioned projects indicate that the utmost attention should be dedicated to the riders' acceptability during the development of a new device. In order to minimize any acceptability issue, this category of measuring devices was not further considered in this research.

Helmet based methodologies may have the potential to estimate in real time a fatal/serious injury. These devices, applied to rider helmets, can enable the real-time estimation of the trauma during a crash. However, practical considerations come into play for a widespread adoption of the existing systems. HITs and 6DOF have the necessity to ensure the constant contact of the accelerometers with the head and the utmost attention should be paid by the user while wearing the helmet: a complex usage procedure could limit the adoption of the improved helmet and the presence of the accelerometers on the accessible surface of the helmet could expose them to unintentional damage. GFT exploits sensors attached to the helmet shell, i.e. far from the head, however it has unsatisfactory average absolute errors (up to 40% if a wide variety of impact directions is considered Allison et al., 2015). To remove the drawbacks posed by the placement of the accelerometers, they could be attached to the inner of the helmet shell. The estimation of the head kinematics could be solved dividing the problem into two parts: (1) the estimation of the linear and rotational accelerations of the helmet CoG; (2) the development of a transfer function to estimate the accelerations of the head CoG from the ones of the helmet.

This study explores the possibility to use an existing technology, the 6DOF method, to perform the first step of the procedure. The 6DOF method was implemented in a finite element (FE) model of a motorcyclist helmet, instrumented with sixteen accelerometers. Since the 6DOF method was developed to estimate the acceleration of a rigid body, the main research question is: can the 6DOF method be applied to a motorcycle helmet to estimate its CoG accelerations with a +/-10% of error at each time over the entire time history? If the time history is not reproduced within a tolerable error, can the peak values of the linear and rotational accelerations be estimated with a +/- 10% error?

2. Materials and methods

2.1. Original 6DOF method

The 6DOF measurement device uses 12 accelerometers positioned in orthogonally oriented pairs at 6 different locations (Fig. 1): sensing axis of the accelerometers is tangential to the head and accelerometers are embedded in a padding to guarantee a contact with the head during impacts. In this setup the measured signals represent the head accelerations.

This method predicts both the linear and rotational head accelerations through an iterative optimization of the head equations of motion (1) during the impact:

$$\|a_i\| = \vec{r_{ai}} \cdot \vec{a} + \vec{r_{ai}} \cdot (\vec{\alpha} \times \vec{r}_i) \tag{1}$$

where $\|a_i\|$ is the acceleration measured by each accelerometer, $\vec{a}$ is the head CoG linear acceleration, $\vec{\alpha}$ is the head CoG rotational acceleration, $\vec{r}_i$ is the accelerometer location relative to the head CoG and $\vec{r_{ai}}$ is the orientation of the sensing axis of each accelerometer. The total squared error between the measured and the estimated acceleration at each location is the cost function (2) for the optimization algorithm (Rowson et al., 2011).

$$\sum_{1}^{12} \left(\|a_i\| - \left[\vec{r_{ai}} \cdot \vec{a} + \vec{r_{ai}} \cdot (\vec{\alpha} \times \vec{r}_i) \right] \right)^2 \tag{2}$$

2.2. Updated 6DOF method

The 6DOF device was implemented in a FE model of a motorcyclist helmet. Compared to the original device described in the previous section, the accelerometers were rigidly attached to the inner of the helmet shell, always in orthogonally pairs to measure the helmet accelerations. The sensing axes of the accelerometers were oriented tangentially to the helmet shell. Although the 6DOF method needs only 12 accelerometers placed in pairs at 6 locations, a higher number of locations was considered to investigate possible optimized configurations of the accelerometers, capable to minimize the estimation errors. The 16 most frequently impacted helmet sections (Fig. 2), according to the Motorcycle Accident In Depth Study (MAIDS) (MAIDS, 2009) coding scheme (Fig. 3), were selected based on in-depth crash data (Fig. 4). Each location was selected within a different helmet section. Considering the accelerometer distribution on the helmet (Fig. 2), 16 locations were considered enough for a satisfactory spatial sampling of the helmet surface.

The same cost function of the original 6DOF device was used to estimate the accelerations, but helmet CoG accelerations were used instead of head CoG accelerations in Eq. (3). The particle swarm algorithm (PSA) was applied as optimization algorithm in this study, versus the simulated annealing (SA) used in the original 6DOF formulation, since PSA has higher performance than SA (Bagaram, 2017).

The 6 pairs of accelerometers required by the 6DOF system were chosen among the 16 pairs of accelerometers available in order to obtain different configurations of accelerometers to be investigated. Two sets of accelerometer configurations were created, based on two different criteria. The selection procedure was a sequential implementation of the following steps:

1. each position was once selected as the first position for a configuration of accelerometers;
2. the remaining five positions were chosen implementing one of the two following criteria:

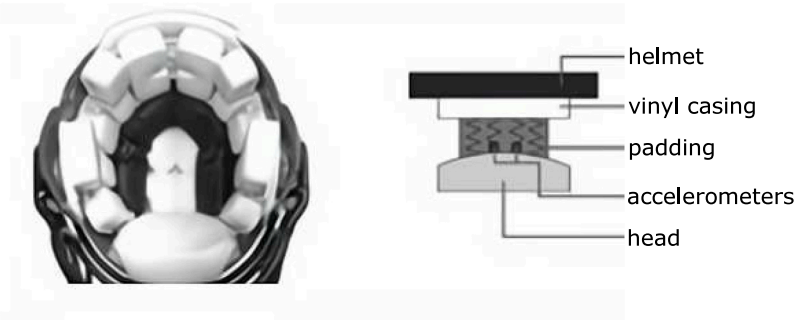

Fig. 1. 6DOF measurement device installed in a Riddell Revolution helmet (left) and a schematic of the measurement device in the helmet (right) (Rowson et al., 2011).

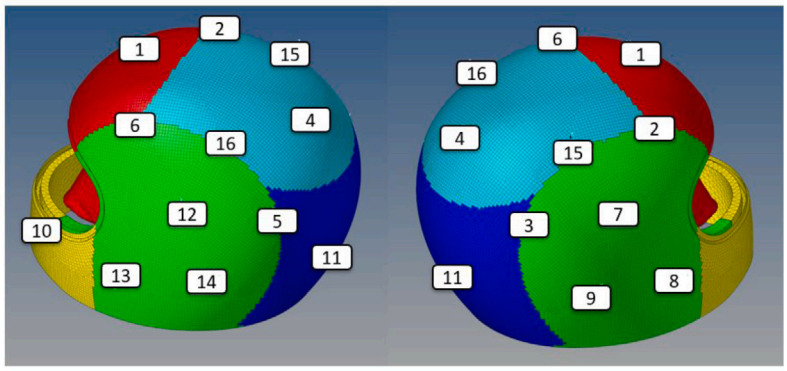

Fig. 2. Locations of the 16 orthogonally oriented accelerometer pairs.

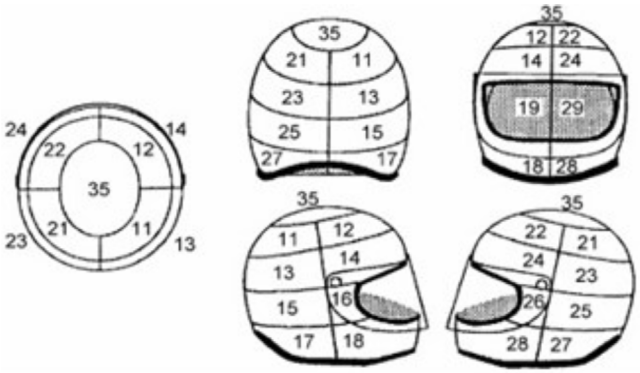

Fig. 3. Coding scheme of helmet sections used in MAIDS (MAIDS, 2009).

(a) maximizing the sum of the distances between any two positions in the configuration (criterion of maximum dispersion);
(b) minimizing the mean square error of the distance between any two accelerometers of the configuration referred to the mean distance among positions in the configuration (criterion of the uniform distribution).

The procedure was defined to systematically position the accelerometers on the helmet shell, to better capture its kinematic. Each configuration had to differ from any previously defined one in order to be included in the study. Thirty-two configurations were created and investigated applying the 6DOF method to find the best performing accelerometer arrangement.

2.3. FE models

A full-face model of helmet (AGV X 3000, size 58/59), certified both DOT FMVSS 218 (DOT-FMVSS-218, 1984) and UNECE 22.05 (ECE22.05, 2002), was used for this study. LS-Dyna solver, version 971 (Hallquist et al., 2006), was used to perform impact simulations. The helmet model, provided by Dainese SpA (Cernicchi et al., 2008), consists of an energy-absorbing liner, an outer shell and a chin strap: shell elements were used for the external polycarbonate shell (material model: MAT058), while solid elements for the expanded polystyrene of the energy-absorbing liner (material model: MAT075). The helmet CoG was connected with an interpolation constraint to 10,000 randomly selected nodes belonging to the shell surface. This modelling of the helmet CoG allowed to measure the reference accelerations while not stiffening the helmet shell. In the impacts, the helmet was coupled with an appropriate rigid headform model.

Three different impact configurations of the helmet on a flat surface were reproduced (Fig. 5). In Configuration 1 the impact point was located on the top of the helmet, while in Configuration 2 the impact point was on the left side of the helmet. These impact configurations were selected to reproduce 2 out of the 5 impact conditions (P and X points) required by the ECE 22.05 standard (ECE22.05, 2002). In the third configuration the impact point was chosen not aligned with the sagittal, transversal or horizontal plane, and the velocity vector was defined to reproduce an oblique impact. In each configuration the helmet impacted the surface at 8 m/s.

The 6DOF algorithm was developed assuming rigid body dynamics, but both the head and helmet are deformable bodies. The helmet shell is a laminated composite, modelled with MAT58 material. To investigate the influence of the helmet deformability on the estimations of the 6DOF algorithm, the elastic Young Modulus of the shell material was progressively increased in a sequence of simulations to approximate the condition of infinitely rigid body. This approach was implemented for the second impact configuration, which presented the largest errors in this study.

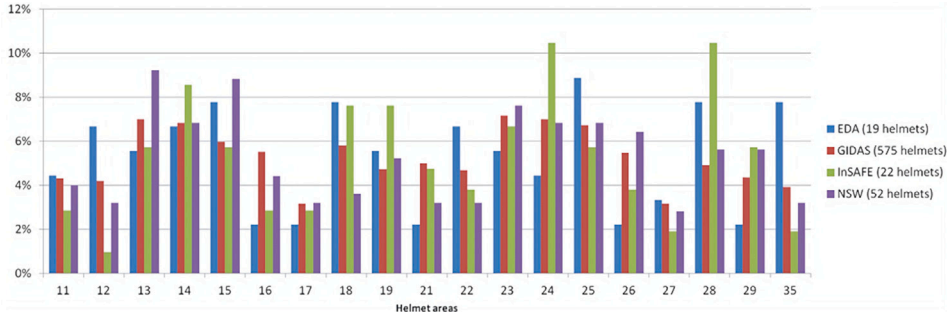

Fig. 4. Distribution of helmet contact sections (EDA, GIDAS, InSAFE, NSW datasets) (Pioneers, 2020) using the MAIDS helmet sections scheme (MAIDS, 2009).

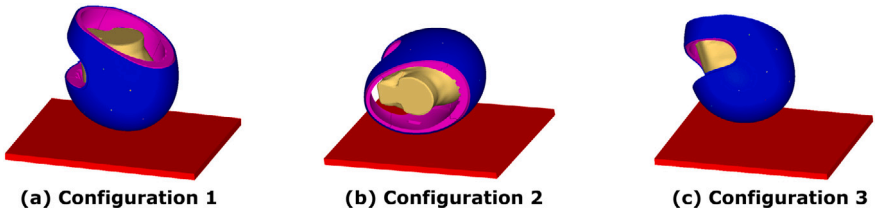

Fig. 5. Impact configurations.

The following metrics were considered to evaluate the error of the computed acceleration: percentage error for linear and angular peak both for resultant and component accelerations; mean and maximum absolute error for the time histories of linear and angular accelerations, both for resultant and each component. In all calculations, the FE helmet CoG accelerations, obtained from the simulations, were taken as reference signals.

Eq. (3) was used to evaluate the mean relative error: ε_{mean} is the mean relative error, n is the number of discrete data points, $6dof$ is the predicted acceleration by the 6DOF method, HF is the reference signal, HF_{max} is the maximum absolute value of the reference signal. A specific HF_{max} was determined for each component and for the resultant of both linear and rotational acceleration. Eq. (4) was used to evaluate the maximum relative error; where ε_{max} is the maximum relative error. Eq. (5) and (6) were used to calculate the peak relative positive and negative errors: ε_{peak-} is the negative one and ε_{peak+} is the positive one; $6dof_{(-)}$ is the negative peak value for the predicted acceleration and $HF_{(-)}$ for the real one (5). Instead, the positive peaks are specified by the plus sign (6).

$$\varepsilon_{mean} = \frac{1}{n}\sum \frac{6dof_i - HF_i}{HF_{max}} \tag{3}$$

$$\varepsilon_{max} = max\left(\frac{6dof_i - HF_i}{HF_{max}}\right) \tag{4}$$

$$\varepsilon_{peak(-)} = \frac{6dof_{(-)} - HF_{(-)}}{HF_{max}} \tag{5}$$

$$\varepsilon_{peak(+)} = \frac{6dof_{(+)} - HF_{(+)}}{HF_{max}} \tag{6}$$

For each configuration of accelerometers, average ε_{mean} and ε_{peak+} over the three impact configurations were computed for both the linear and rotational resultant accelerations. The accelerometer configuration that minimized both the errors was selected as the best one. Specifically, ε_{mean} was used to understand if this method was suitable to reproduce the entire time history of the acceleration of the helmet CoG; instead, ε_{peak+} gave an estimation of the method performances in the prediction of peak values.

3. Results

The first step was to identify and select the best relative position of accelerometers among the 32 configurations defined in the previous section. According to the results in Tables 1 and 2, the configurations of accelerometers obtained maximizing the distance between each accelerometer locations are characterized by lower values for both the average ε_{mean}, ε_{max} and average ε_{peak+}. Among these configurations, ε_{mean} has similar values both for the resultant linear acceleration and the resultant rotational acceleration (Table 1). Moreover, most of these configurations have average ε_{peak+} below 5% for the resultant linear acceleration. As the average ε_{peak+} for the resultant rotational acceleration and ε_{max} for both the linear and rotational accelerations are the error metrics with the largest values, the best configuration had to minimize these parameters. The selected configuration (#4) is also characterized by the best value of the average ε_{mean} both for the resultant linear and rotational accelerations. It includes the sensors located at the positions 1-4-8-10-11-13 (Fig. 2). The configuration was used for the performance assessment of the 6DOF method in the estimation of the helmet CoG accelerations.

For each configuration the comparison was performed at component level and the related errors metrics were computed and analysed. In the first configuration (Figs. 6 and 7) the most relevant discrepancies occur in a_x and a_y linear accelerations and in α_x and α_z rotational accelerations. The impact kinematics is mainly along the Z axis and around the Y axis. Therefore, a_z and α_y are the components with larger amplitude and a good qualitative match can be observed. The errors reported in Table 3 confirm the qualitative assessment: the positive and negative peak values of the linear acceleration along the Z axis and the resultant amplitude are estimated almost perfectly (maximum error 1%). Both the a_z and the resultant linear acceleration are characterized by larger values of ε_{max} (respectively 16% and 17%). In the graphs of Figs. 6 and 7, components (a_z and α_y), the differences between the reference and predicted data increase shortly after the main peak (starting from 0.015 s). Instead, the component along the X axis is characterized by the worst estimation as underlined by the maximum relative error equal to 23% and the negative and positive peak errors equal to 12% and 9%.

Similar results were obtained for the rotational acceleration, although errors are larger than for the linear acceleration: the main component (α_y) and the resultant are characterized by the smallest peak estimation errors. Instead, the resultant rotational acceleration has the worst ε_{max} equal to 50% due to the high ε_{max} values of the three components. Without the presence of a marked peak in the acceleration

Table 1
Average ϵ_{mean}, ϵ_{max} and ϵ_{peak+} over the three impact configurations as a function of the 16 accelerometer configurations obtained maximizing the distance between each accelerometer location.

Error Type	*Acceleration Type*	*Accelerometer configurations*															
		1	*2*	*3*	*4*	*5*	*6*	*7*	*8*	*9*	*10*	*11*	*12*	*13*	*14*	*15*	*16*
ϵ_{mean} [%]	*Linear*	5.06	5.67	5.17	4.49	4.95	4.22	5.03	5.13	4.62	4.90	4.41	4.15	5.17	5.42	4.65	5.11
	Rotational	12.1	14.0	14.0	12.2	14.5	13.7	14.0	14.4	14.2	13.4	13.2	12.8	13.7	14.5	13.2	14.5
ϵ_{max} [%]	*Linear*	40.8	37.2	42.7	42.3	42.5	32.2	31.0	40.1	39.1	39.4	41.7	35.7	35.5	44.8	36.3	31.4
	Rotational	93.5	125	101	83.1	117	120	110	125	93.3	103	100	95.9	107	116	93.0	115
ϵ_{peak+} [%]	*Linear*	9.29	3.91	1.32	3.25	5.00	2.37	13.2	5.49	3.05	13.5	1.97	1.70	8.64	9.87	4.46	2.91
	Rotational	40.3	59.0	34.2	30.7	45.3	48.0	60.5	49.0	44.3	45.5	34.4	32.4	61.1	46.1	34.1	58.5

Table 2
Average ϵ_{mean}, ϵ_{max} end ϵ_{peak+} over the three impact configurations as a function of the 16 accelerometer configurations obtained minimizing the mean square error of the mean distance between each accelerometer location.

Error Type	*Acceleration Type*	*Accelerometer configurations*															
		1	*2*	*3*	*4*	*5*	*6*	*7*	*8*	*9*	*10*	*11*	*12*	*13*	*14*	*15*	*16*
ϵ_{mean} [%]	*Linear*	11.3	10.5	10.5	8.24	9.42	10.6	10.8	11.7	10.6	9.96	10.5	9.29	7.08	10.1	10.0	10.7
	Rotational	33.0	34.5	33.1	31.6	30.7	31.1	33.7	32.9	33.3	31.1	32.3	31.0	25.4	32.3	33.9	28.2
ϵ_{max} [%]	*Linear*	74.6	67.1	72.2	42.3	63.3	72.9	80.2	87.2	79.6	68.9	65.7	60.6	39.6	71.0	62.4	88.1
	Rotational	203	234	212	234	212	189	198	197	191	205	202	218	185	219	228	178
ϵ_{peak+} [%]	*Linear*	27.8	26.1	31.4	7.99	15.7	26.1	39.1	45.9	39.2	23.1	19.7	15.8	13.7	24.8	13.1	44.2
	Rotational	139	171	151	170	147	126	166	129	157	140	137	153	119	154	163	104

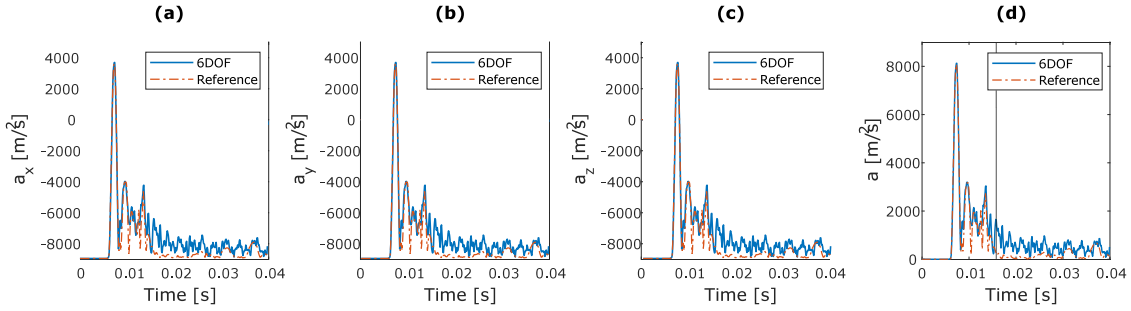

Fig. 6. Configuration 1: response of the simulated and 6DOF estimated linear accelerations of the helmet CoG (see also Table 3): (a) x axis component, (b) y axis component, (c) z axis component, (d) resultant acceleration. The vertical line indicates the time corresponding to ϵ_{max}.

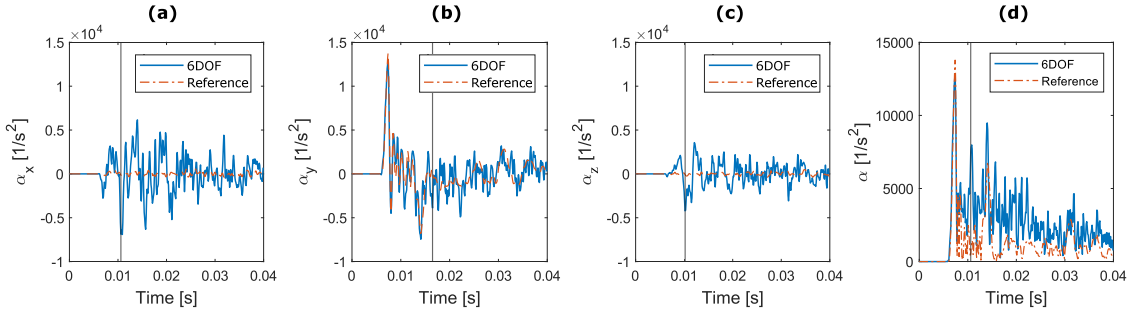

Fig. 7. Configuration 1: response of the simulated and 6DOF estimated rotational accelerations of the helmet CoG (see also Table 3): (a) x axis component, (b) y axis component, (c) z axis component, (d) resultant acceleration. The vertical line indicates the time corresponding to ϵ_{max}.

Table 3
Configuration 1: mean and maximum relative errors, positive and negative peak errors for the helmet accelerations.

Error type	Linear Acceleration				Rotational Acceleration			
	a_x	a_y	a_z	Resultant	α_x	α_y	α_z	Resultant
ϵ_{mean} [%]	3.67	0.89	3.41	4.01	10.4	6.98	5.57	10.2
ϵ_{max} [%]	22.6	6.57	15.5	17.3	48.7	30.4	29.9	49.7
ϵ_{peak+} [%]	8.51	3.81	0.82	0.60	40.4	8.80	22.3	8.05
ϵ_{peak-} [%]	11.8	5.50	0.41	/	46.6	4.64	26.8	/

Note: / is used when the parameter is not applicable.

signal, the 6DOF algorithm was not able to properly predict both α_x and α_z (Fig. 7).

In the second configuration, the helmet velocity was aligned with the Y axis and the helmet impacted the surface on the right side. The

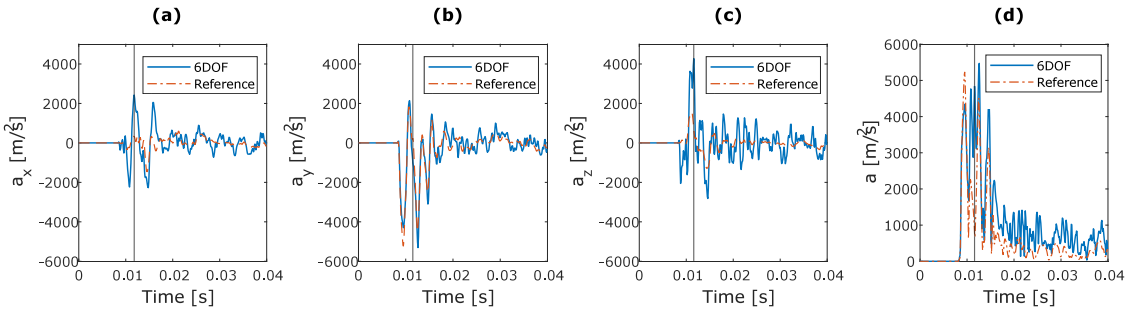

Fig. 8. Configuration 2: response of the simulated and 6DOF estimated linear accelerations of the helmet CoG (see also Table 4): (a) x axis component, (b) y axis component, (c) z axis component, (d) resultant acceleration. The vertical line indicates the time corresponding to ϵ_{max}.

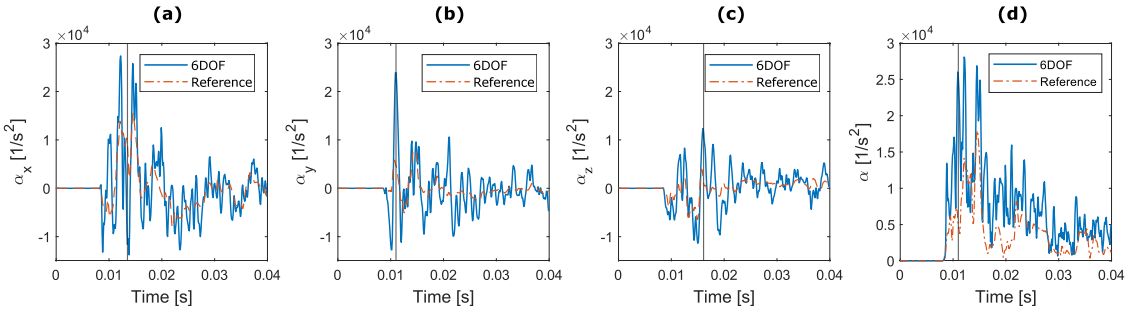

Fig. 9. Configuration 2: response of the simulated and 6DOF estimated rotational accelerations of the helmet CoG (see also Table 4): (a) x axis component, (b) y axis component, (c) z axis component, (d) resultant acceleration. The vertical line indicates the time corresponding to ϵ_{max}.

Table 4
Configuration 2: mean and maximum relative errors, positive and negative peak errors for the helmet accelerations.

Error type [%]	Linear Acceleration				Rotational Acceleration			
	a_x	a_y	a_z	Resultant	α_x	α_y	α_z	Resultant
ϵ_{mean} [%]	6.34	4.73	8.46	8.63	17.8	13.6	10.6	18.3
ϵ_{max} [%]	39.9	23.0	68.1	77.7	115	107	57.7	113
ϵ_{peak+} [%]	34.9	5.94	51.9	4.48	65.7	88.4	46.7	56.2
ϵ_{peak-} [%]	15.2	1.29	29.2	/	31.2	42.7	27.2	/

Note: / is used when the parameter is not applicable.

6DOF estimations show more diffuse errors, but the linear acceleration along the Y axis has been correctly estimated (Fig. 8). All the predicted components of the rotational acceleration differ from the reference curves (Fig. 9). Overall, the curves predicted by the 6DOF system tend to overestimate the local maxima and minima of the acceleration components. The errors confirm these findings (Table 4). a_y is the only component of acceleration predicted with acceptable errors: 6% and 1% for ϵ_{peak+} and ϵ_{peak-} respectively, while ϵ_{mean} is 5%. The other components of the linear acceleration have errors up to 52% in the estimation of the positive peak value and 29% for the negative one of a_z. The resultant linear acceleration shows a small error on the peak value ($\epsilon_{peak+} = 4\%$), although the time history does not reproduce the reference curve. The peak value of the target acceleration occurred at $t_1 = 0.009$ s, instead in the acceleration reproduced with the 6DOF the peak occurred at $t_2 = 0.012$ s. All the estimated rotational acceleration components show significant errors: up to 88% in the estimation of the positive peak value of α_y and ϵ_{mean} in the range 11%–17%. The resultant rotational acceleration has similar results for ϵ_{mean} (18%) and ϵ_{peak+} (56%). In Fig. 9 the rotational accelerations are compared. The average mean and maximum relative errors are 15% ± 4% and 98% ± 30% respectively; while the average positive peak error is 64% ± 21% and the average negative peak error is 34% ± 8%. The whole results are reported in the Table 4.

In the third configuration a generic impact, with randomly selected direction of the helmet velocity and helmet orientation with respect to the plate, was reproduced. The linear and rotational accelerations, components and resultants, are reported in Figs. 10 and 11. Y and Z components of the linear accelerations have similar amplitudes and they show a good agreement with the reference signals. X component has a smaller amplitude range, but it shows a comparable qualitative match between 6DOF and reference curves. Results reported in Table 1 confirm the previous analysis: the ϵ_{mean} does not exceed 4% for each component. Peak errors show that a_x and a_y have the best negative (ϵ_{peak-}), and positive (ϵ_{peak+}) peak predictions. The quality of the component estimation also affected the resultant estimation as demonstrated by ϵ_{mean} and ϵ_{peak+}, respectively equal to 4% and 5%.

The prediction of the rotational accelerations is still affected by a greater error than the linear acceleration (Table 5): ϵ_{mean} never falls below 10% and errors up to 70% and 73% affect respectively the positive and negative peak estimations. The comparison between the predicted and target rotational accelerations is shown in Fig. 11. 6DOF curves tend to overestimate local minima and maxima of the real acceleration over the entire time history, leading to unacceptable errors in estimation as discussed above.

The 6DOF measurement device was developed to be used with substantially rigid body, but in this study the accelerometers were attached to the helmet shell, a deformable body. The impact configuration with the prediction performances of the worst accelerations, i.e. the second configuration, was selected as test case to verify how deformability affected the results. Increments from 10 to 10^4 times of the helmet shell Young modulus were implemented to change the deformability of the body up to an extremely stiff shell. Results shown in Table 6

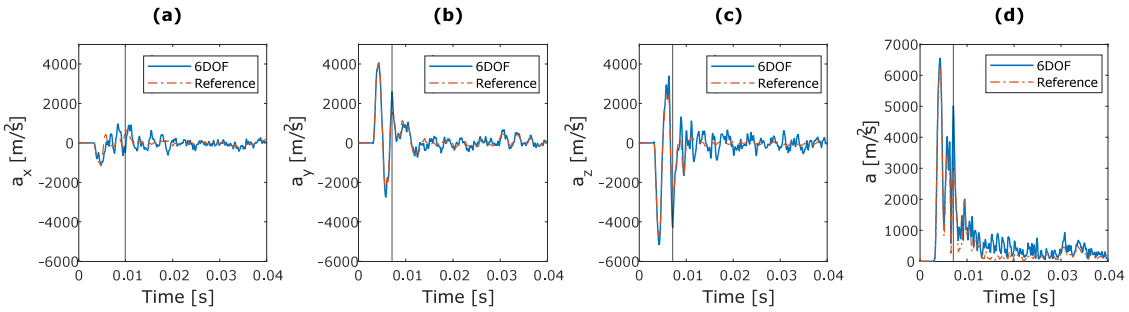

Fig. 10. Configuration 3: response of the simulated and 6DOF estimated linear accelerations of the helmet CoG (see also Table 5): (a) x axis component, (b) y axis component, (c) z axis component, (d) resultant acceleration. The vertical line indicates the time corresponding to ϵ_{max}.

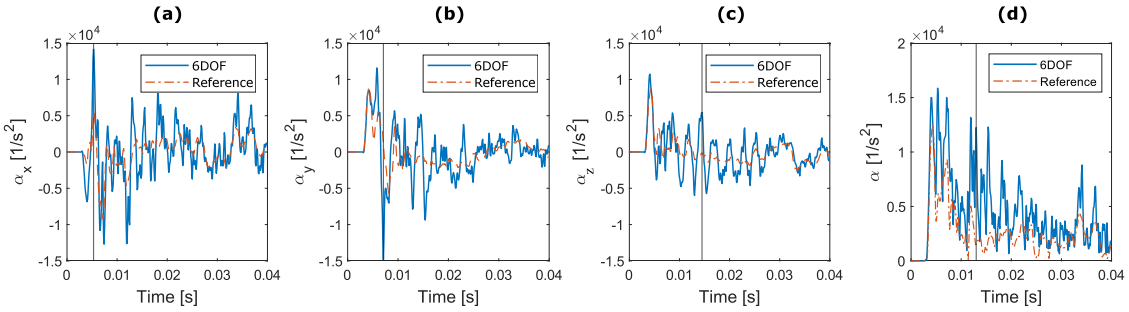

Fig. 11. Configuration 3: response of the simulated and 6DOF estimated rotational accelerations of the helmet CoG (see also Table 5): (a) x axis component, (b) y axis component, (c) z axis component, (d) resultant acceleration. The vertical line indicates the time corresponding to ϵ_{max}.

Table 5
Configuration 3: mean and maximum relative errors, positive and negative peak errors for the helmet accelerations.

Error type [%]	Linear Acceleration				Rotational Acceleration			
	a_x	a_y	a_z	Resultant	α_x	α_y	α_z	Resultant
ϵ_{mean} [%]	2.91	1.64	4.04	3.82	15.2	14.4	11.0	17.1
ϵ_{max} [%]	14.4	16.5	27.2	31.9	72.4	129	45.0	86.5
ϵ_{peak+} [%]	4.74	0.89	12.3	4.68	69.9	21.2	16.2	27.8
ϵ_{peak-} [%]	0.75	7.14	6.86	/	27.5	73.4	27.6	/

Note: / is used when the parameter is not applicable.

highlighted a decreasing trend in the four error metrics as the stiffness of the helmet shell increased: ϵ_{mean} decreased in the range 1%–2% and 5%–6% respectively for the linear and rotational accelerations; ϵ_{max} showed the greatest improvement (e.g. the related error of α_x decreased from 115% to 32%); both ϵ_{peak+} and ϵ_{peak-} dropped below 15%.

4. Discussion

eCall is a pan-European system for the automatic emergency call in case of road crashes. Initially developed for cars, eCall was extended to other vehicles, including Powered Two-Wheelers (PTWs), within the I_Heero project. Currently BMW is offering the system on its motorcycles but also aftermarket systems are available. This technology on PTWs enables new possibilities for early crash detection and emergency treatment of riders. In fact, riders are not protected by an outer structure as in cars, but the helmet use is mandatory in several countries. Helmet could be turned into a sensing protective equipment, capable to improve the crash detection (currently performed by on-board sensors) but also to integrate a real time estimation of head injuries into the activation criterion of the eCall. The latter data could also be transmitted to the rescue team and enable a more timely and effective intervention. TBIs are overrepresented among riders (Gibson and Thai, 2007), and they are one of the most severe and dangerous consequences of an impact. Detection and timely treatment are key to minimize consequences (Tepas III. et al., 2009).

The estimation of head injuries requires appropriate knowledge of the head kinematics during the impact. Measurement systems embedded into the helmets could provide adequate data to perform real time estimation of the injuries, but new helmets should require to the end users the same level of usage expertise than the current marketed solutions. As the 6DOF method has strict requirements for the positioning of sensors (i.e. in contact with the head), there is the need to investigate possible changes to sensors layout and the implications on the accuracy and precision of the derived data. In the current study the sensors were attached to the inner side of the outer shell of the helmet.

From 16 pairs of accelerometers, 32 possible configurations of the sensors were defined and simulated in the three impact configurations, representative of crash conditions both in terms of impact points and velocity. The accelerometer configurations obtained with the maximization of the distance between accelerometer locations (Table 1) led to better accuracy than minimizing the square error referred to the mean distance (Table 2). On the contrary, the accelerometer configurations generated with the same criterion had similar performances and none of them was clearly outperforming the other ones. For instance, the sixteen accelerometer configurations in Table 1 have comparable values of ϵ_{mean} both for the linear and rotational accelerations. Similar remarks apply to ϵ_{max}, except that some configurations (#2, #6, #8) have noticeably higher values. The results demonstrate the strong effect of the criterion for the sensor distribution on the prediction accuracy of CoG accelerations with flexible bodies, and negligible differences among the accelerometer configurations generated with

Table 6
Increasing Young modulus of the outer shell: mean and maximum relative errors, positive and negative peak errors for the helmet accelerations.

Error type	Configuration	Linear Acceleration				Rotational Acceleration			
		a_x	a_y	a_z	Resultant	α_x	α_y	α_z	Resultant
ϵ_{mean} [%]	E	6.34	4.73	8.46	8.63	17.8	13.6	10.6	18.3
	$E*10$	4.52	2.51	4.15	4.58	6.37	5.48	5.85	6.85
	$E*10^2$	3.37	2.45	3.72	3.87	11.3	8.10	9.23	11.3
	$E*10^3$	2.13	1.92	2.98	3.27	7.98	5.64	7.23	7.45
	$E*10^4$	1.18	1.20	1.80	1.88	6.46	4.51	4.89	5.00
ϵ_{max} [%]	E	40.0	23.0	68.1	77.7	115	107	57.7	113
	$E*10$	34.4	14.6	33.0	34.6	60.9	46.3	37.3	45.9
	$E*10^2$	19.3	12.7	36.9	20.2	56.6	52.7	54.8	54.0
	$E*10^3$	11.2	10.0	28.7	14.8	37.3	30.3	60.1	45.9
	$E*10^4$	5.14	5.49	13.0	7.65	32.4	26.1	25.9	25.5
ϵ_{peak+} [%]	E	34.9	5.93	51.9	4.49	65.7	88.4	46.7	56.2
	$E*10$	23.8	12.2	22.3	12.0	5.14	27.4	26.6	17.3
	$E*10^2$	8.60	4.44	18.0	6.38	30.9	22.8	28.1	27.4
	$E*10^3$	8.34	1.43	28.3	2.09	32.7	13.3	17.3	30.5
	$E*10^4$	0.67	4.54	12.2	5.92	0.39	10.2	12.1	8.17
ϵ_{peak-} [%]	E	15.2	1.29	29.2	/	31.1	42.7	27.2	/
	$E*10$	30.3	14.6	16.1	/	23.6	34.4	21.4	/
	$E*10^2$	15.4	9.52	21.7	/	31.6	30.2	32.3	/
	$E*10^3$	5.42	2.12	13.0	/	19.0	18.2	17.7	/
	$E*10^4$	3.58	4.62	5.55	/	6.62	14.8	11.1	/

Note: / is used when the parameter is not applicable.

the same criterion. The observed differences may vanish if the accelerometer configurations would be tested on a larger set of impact configurations. Such a test should be conducted before accepting the possibility to successfully perform an optimization of the accelerometer distribution within a specific distribution criterion. This activity was not developed within the present research, since the main focus was on the applicability of the 6DOF method to flexible bodies. Nonetheless the following research activities were developed with the best accelerometer configuration, i.e. #4 in Table 1, as it minimized the greatest number of errors metrics (i.e. 4 out of 6).

The system, with the selected accelerometer configuration, was tested in three different impact configurations. The results show a good capability in the assessment of linear acceleration peak values: in all configurations the peak error on the resultant of the linear acceleration never exceeded 5%, although in the second configuration the peak of the 6DOF prediction was delayed compared to the reference signal. The latter result is a consequence of higher peak errors in the components: maximum peak error exceeded 50% in this configuration, while it reached 12% in the other two configurations. In general, the 6DOF prediction of the linear accelerations overestimated the local minima and maxima in each impact configuration (Tables 3–5). This trend was extremely evident in the second impact configuration time histories of the x and z components as well as for the resultant (Fig. 8). The predicted signals were good in proximity of the peaks of the resultant for the configurations 1 and 3 as well as of the components with the largest amplitude for all impact configurations, but they failed to match the reference signals over the entire time range.

With reference to the rotational acceleration, the results highlighted the general difficulty of the method to correctly reproduce the entire time history of the in each component. Specifically, the predicted rotational accelerations tended to overestimate the local minima and maxima as for the linear accelerations. Mean errors were never below 6% in any impact configuration, with a maximum of 18% in the estimation of the resultant rotational acceleration in the second impact configuration, and the predicted values of the negative and positive peaks had errors up to 88%.

The results demonstrated an extremely limited predictive capability for the 6DOF method applied to a flexible body, already in a limited set of impact configurations. The errors were not in line with the desired accuracy and they did not justify further investigation. In fact, this research aimed to verify the general applicability of the 6DOF method to predict the CoG accelerations of a flexible body. The parametric study on the elasticity of the outer shell, confirmed that the main source of error is the body deformability.

An intrinsic limitation applies to this study. Namely the impossibility of carrying out an experimental verification, as the CoG is not a physical point of the helmet and no measurement of its accelerations can be performed. A secondary possible limitation could be the use of a single helmet model. Nonetheless the feasibility study is not affected by this limitation, as more helmets would be necessary to confirm a positive estimation capability of the 6DOF method but a single helmet is sufficient to prove the limitations, if a general application of the method is desired.

This research showed that a different method has to be identified for the prediction of the CoG accelerations. Such a method should be capable of handling the flexibility of the body and, possibly, it should also integrate the transfer function from the CoG accelerations of the helmet to the head accelerations.

5. Conclusions

The study focused on the investigation of the 6DOF method to estimate the acceleration of a motorcyclists' helmet centre of gravity. Three different configurations of a helmet, coupled with a standard rigid head and impacting on a deformable plate, were reproduced in a virtual environmental. The FE model of the helmet was integrated with 32 accelerometers in orthogonally pairs at 16 different locations on its outer shell.

Since the 6DOF needed only 6 pairs of accelerometers, a preliminary study to identify the best configuration of accelerometers was performed. The criterion used to generate the accelerometer configurations influenced the precision of the estimated results, but there were limited differences among the best configurations based on the same criterion. The best configuration was used for a detailed analysis and comparison of the predicted signals with the reference ones.

Results suggested that the 6DOF capability to estimate linear accelerations depended on the impact configuration and on the desired outcome. If the peak of the resultant linear acceleration could suffice, the investigation on the 6DOF applicability to flexible bodies could be further extended. If the prediction of the entire acceleration signal

is sought, the 6DOF method has severe limitations, especially for the rotational accelerations.

Future works should consider a totally novel method capable of taking into account the flexibility of the body, which is the greatest limit of technologies integrated into the helmet. Otherwise, a novel technology able to directly estimate the head CoG accelerations using sensors attached to the helmet surface should be deepened.

CRediT authorship contribution statement

A. Bracali: Conceptualization, Methodology, Software, Formal analysis, Data curation, Writing – original draft, Writing – review & editing. **D. Barbani:** Conceptualization, Methodology, Writing – review & editing, Supervision. **N. Baldanzini:** Conceptualization, Methodology, Writing – review & editing, Supervision.

Declaration of competing interest

The authors declare that they have no known competing financial interests or personal relationships that could have appeared to influence the work reported in this paper.

Acknowledgement

Authors acknowledge the Dainese SpA for the support in FE modelling.

References

Aare, M., Holst, H., 2003. Injuries from motorcycle- and moped crashes in Sweden from 1987 to 1999. Inj. Control Saf. Promot. 10 (3), 131–138.

Allison, M.A., Kang, Y.S., Maltese, M.R., Bolte, J.H., Arbogast, K.B., 2015. Measurement of hybrid III head impact kinematics using an accelerometer and gyroscope system in ice hockey helmets. Ann. Biomed. Eng. 43 (8), 1896–1906. http://dx.doi.org/10.1007/s10439-014-1197-z.

Bagaram, M., 2017. Comparison of Simulated Annealing and Particle Swarm Optimization on Reliability-Redundancy Problem (Ph.D. thesis). University Of Washington.

Beckwith, J.G., Chu, J.J., Greenwald, R.M., 2007. Validation of a noninvasive system for measuring head acceleration for use during boxing competition. J. Appl. Biomech. 23 (3), 238–244. http://dx.doi.org/10.1123/jab.23.3.238.

Beckwith, J.G., Greenwald, R.M., Chu, J.J., 2012. Measuring head kinematics in football: Correlation between the head impact telemetry system and hybrid III headform. Ann. Biomed. Eng. 40 (1), 237–248. http://dx.doi.org/10.1007/s10439-011-0422-2.

Bekiaris, E.D., Spadoni, A., Nikolaou, S.I., 2009. SAFERIDER project: new safety and comfort in powered two wheelers. In: 2009 2nd Conference on Human System Interactions. IEEE, pp. 600–602.

Centers for Disease Control and Prevention, et al., 2014. Traumatic brain injury in the United States: Fact sheet. Washington, DC: Centers for Disease Control and Prevention.

Cernicchi, A., Galvanetto, U., Iannucci, L., 2008. Virtual modelling of safety helmets: practical problems. Int. J. Crashworth. 13 (4), 451–467.

Chinn, B., Canaple, B., Derler, S., Doyle, D., Otte, D., Schuller, E., Willinger, R., 2001. Cost 327 motorcycle safety helmets. European Commission, Directorate General for Energy and Transport.

Chu, J.J., 2005. An algorithm for estimating acceleration magnitude and impact location using multiple nonorthogonal single-axis accelerometers. J. Biomech. Eng. 126 (6), 849. http://dx.doi.org/10.1115/1.1824135.

Crisco, J.J., Wilcox, B.J., Beckwith, J.G., Chu, J.J., Duhaime, A.C., Rowson, S., Duma, S.M., Maerlender, A.C., McAllister, T.W., Greenwald, R.M., 2011. Head impact exposure in collegiate football players. J. Biomech. 44 (15), 2673–2678. http://dx.doi.org/10.1016/j.jbiomech.2011.08.003.

Delhaye, A., Marot, L., 2015. A European scanning tour for motorcycling safety, final report of the EC/MOVE/C4 project RIDERSCAN.

DOT-FMVSS-218, 1984. Laboratory procedure for motorcycle helmet testing - federal motor vehicle safety standard no. 218. National Highway Traffic Safety Administration, Department of Transportation U.S..

ECE22.05, 2002. Uniform provisions concerning the approval of protective helmets and of their visors for drivers and passengers.

EuroNCAP, 2017a. European New car assessment programme (Euro NCAP) assessment protocol adult occupant protection. November.

EuroNCAP, 2017b. European New car assessment programme (Euro NCAP) pedestrian testing protocol. November.

Funk, J.R., Duma, S.M., Manoogian, S.J., Rowson, S., 2007. Biomechanical risk estimates for mild traumatic brain injury. J. Chem. Inf. Model. 51 (9), 343–361. http://dx.doi.org/10.1017/CBO9781107415324.004.

Gabler, L.F., Huddleston, S.H., Dau, N.Z., Lessley, D.J., Arbogast, K.B., Thompson, X., Resch, J.E., Crandall, J.R., 2020. On-field performance of an instrumented mouthguard for detecting head impacts in American football. Ann. Biomed. Eng. 48 (11), 2599–2612.

Gennarelli, T.A., Thibault, L.E., Ommaya, A.K., 1972. Pathophysiologic Responses to Rotational and Translational Accelerations of the Head. SAE Technical Papers, pp. 296–308. http://dx.doi.org/10.4271/720970.

Gibson, T., Thai, K., 2007. Helmet Protection Against Basilar Skull Fracture. ATSB Research and Analysis Report, Citeseer.

Greenwald, R.M., Joseph, T.G., Chu, J.J., Crisco, J.J., 2008. Head impact severity measures for evaluating brain injury risk exposure. pp. 789–798. http://dx.doi.org/10.1227/01.NEU.0000311244.05104.96, 62, 4.

Hallquist, J.O., et al., 2006. LS-DYNA theory manual. Livermore Softw. Technol. Corp. 3, 25–31.

Jadischke, R., Viano, D.C., Dau, N., King, A.I., McCarthy, J., 2013. On the accuracy of the head impact telemetry (hit) system used in football helmets. J. Biomech. 46 (13), 2310–2315. http://dx.doi.org/10.1016/j.jbiomech.2013.05.030.

Kimpara, H., Nakahira, Y., Iwamoto, M., 2011. Head injury prediction methods based on 6 degree of freedom head acceleration measurements during impact. Int. J. Automot. Eng. 2 (2), 13–19. http://dx.doi.org/10.20485/jsaeijae.2.2_13.

Kleiven, S., 2006. Evaluation of head injury criteria using a finite element model validated against experiments on localized brain motion, intracerebral acceleration, and intracranial pressure. Int. J. Crashworthiness 11 (1), 65–79. http://dx.doi.org/10.1533/ijcr.2005.0384.

Knox, T., 2002. Use of Instrumented Earplugs to Measure Driver Head Accelerations. SAE Technical Paper.

MAIDS, 2009. In-Depth Investigations of Accidents Involving Powered Two-Wheelers. Final Report 2.0 [Report]. - [s.l.], Association of European Motorcycle Manufacturers (ACEM.

Majdan, M., Mauritz, W., Wilbacher, I., Janciak, I., Brazinova, A., Rusnak, M., Leitgeb, J., 2012. Traumatic brain injuries caused by traffic accidents in five European countries: outcome and public health consequences. Eur. J. Public Health 23 (4), 682–687. http://dx.doi.org/10.1093/eurpub/cks074.

Melvin, J., 1991. Review of biomechanical impact response and injury in the automotive environment. Transportation Research Circular.

Meng, S., Cernicchi, A., Kleiven, S., Halldin, P., 2020. High-speed helmeted head impacts in motorcycling: A computational study.

Miller, L.E., Kuo, C., Wu, L.C., Urban, J.E., Camarillo, D.B., Stitzel, J.D., 2018. Validation of a custom instrumented retainer form factor for measuring linear and angular head impact kinematics. J. Biomech. Eng. 140 (5).

Newman, J.A., 1986. A generalized model for brain injury threshold. In: Proceedings of International Conference on the Biomechanics of Impact, 1986. pp. 121–131.

Newman, J.A., Shewchenko, N., Welbourne, E., 2000. A proposed new biomechanical head injury assessment function -the maximum power index. Reprinted from: Stapp Car Crash J. 44 (724).

Pioneers, 2020. D1.1 powered two-wheelers – road traffic accidents scearios and common injuries, protective innovations of new equipment for enhanced rider safety.

Rowson, S., Beckwith, J.G., Chu, J.J., Leonard, D.S., Greenwald, R.M., Duma, S.M., 2011. A six degree of freedom head acceleration measurement device for use in football. J. Appl. Biomech. 27 (1), 8–14.

Rowson, S., Duma, S.M., Beckwith, J.G., Chu, J.J., Greenwald, R.M., Crisco, J.J., Brolinson, P.G., Duhaime, A.C., McAllister, T.W., Maerlender, A.C., 2012. Rotational head kinematics in football impacts: An injury risk function for concussion. Ann. Biomed. Eng. 40, http://dx.doi.org/10.1007/s10439-011-0392-4.

S.M., D., S.J., M., W.R., B., P.G., B., M.W., G., J.J., D., R.M., G., J.J., C., J.J., C., 2005. Analysis of real-time head accelerations in collegiate football players. Clin. J. Sport Med. 15 (1), 3–8.

Takhounts, E.G., Eppinger, R.H., Campbell, J.Q., Tannous, R.E., Power, E.D., Shook, L.S., 2003. On the Development of the SIMon Finite Element Head Model. SAE Technical Papers, 2003-October, October, pp. 107–133. http://dx.doi.org/10.4271/2003-22-0007.

Tepas III., J.J., Leaphart, C.L., Pieper, P., Beaulieu, C.L., Spierre, L.R., Tuten, J.D., Celso, B.G., 2009. The effect of delay in rehabilitation on outcome of severe traumatic brain injury. J. Pediatr. Surg. 44 (2), 368–372.

Thomas, A., Gennarelli, M., Lawrence, E., Thibault, S.D., 1982. Biomechanics of Acute Subdural Hematoma. J. Trauma. 680–686.

Tierney, R.T., Higgins, M., Caswell, S.V., Brady, J., McHardy, K., Driban, J.B., Darvish, K., 2008. Sex differences in head acceleration during heading while wearing soccer headgear. J. Athl. Train. 43 (6), 578–584.

Versace, J., 1971. A review of the severity index.